Imaging and Analysis Techniques for Electrical Trees using X-ray Computed Tomography

Roger Schurch[1,2], Simon M. Rowland[1], Robert S. Bradley[3] and **Philip J. Withers[3]**
[1]School of Electrical and Electronic Engineering, University of Manchester, Manchester, United Kingdom
[2]Department of Electrical Engineering, Federico Santa Maria Technical University, Valparaiso, Chile
[3]School of Materials, University of Manchester, Manchester, United Kingdom

ABSTRACT

Electrical treeing is one of the main mechanisms of degradation in polymeric high voltage insulation, a precursor of power equipment failure. Electrical trees have been previously imaged mostly using two-dimensional imaging techniques; thereby loosing valuable information. Here we review the techniques that have been previously used and present the novel application of X-ray computed tomography (XCT) for electrical tree imaging. This non-destructive technique is able to reveal electrical trees, providing a three-dimensional (3-D) view and therefore, a more complete representation of the phenomenon can be achieved. Moreover, taking virtual slices through the replica so created brings the possibility of internal exploration of the electrical tree, without the destruction of the specimen. Here, laboratory created electrical trees have been scanned using XCT with phase contrast enhancement, and 3-D virtual replicas created through which the trees are analyzed. Serial Block-Face scanning electron microscopy (SBFSEM) is shown to be a successful complementary technique. Computed tomography enables quantification of electrical tree characteristics that previously were not available. Characteristics such as the diameter and tortuosity of tree channels, as well as the overall tree volume can be calculated. Through the cross-section analysis, the progression of the number of tree channels and the area covered by them can be investigated. Using this approach it is expected that a better understanding of electrical treeing phenomenon will be developed.

Index Terms — **Electrical trees, Three-dimensional, 3-D, Imaging, X-ray, Tomography, XCT, SEM, SS-SEM, SBFSEM.**

1 INTRODUCTION

THE reliability of high voltage electrical insulation is critical to the quality of national power supplies. Failure of solid polymeric high voltage insulation is commonly a consequence of electrical treeing. Electrical trees are tubular channels of degradation in highly stressed polymeric insulation caused by electrical discharges which, over long periods of time, lead to failure of the insulation. The term 'electrical tree' arises from their shape, which is like a natural tree as shown in Figure 1 [1, 2]. Electrical trees are evidence of a cumulative and irreversible process which may lead to electrical breakdown, and is seen in electrical power equipment, such as power cables, electrical machines, switchgear and transformer bushings [3]. By better understanding the initiation and growth processes of electrical trees, power utilities will be able to improve their asset management, so enhancing network reliability. At the same time, equipment manufacturers and material suppliers will be able to upgrade their product design, reducing cost of infrastructure investments.

Manuscript received on 17 January 2013, in final form 13 August 2013, accepted 13 August 2013.

Electrical treeing in solid insulation has been studied for many years [4]. Nonetheless, the processes are yet to be fully understood, and little can be predicted concerning for example electrical tree initiation or growth rate. In insulation materials in power systems equipment, trees grow over tens of years; however, in the laboratory trees are typically grown over periods of a few hours by enhancing the electrical field. This is normally achieved by generating a high divergent electrical field inside a material, using a sharp needle as an electrode [5]. The sample is constructed so that there is a gap of 2-3 mm between the high voltage electrode (normally the needle) and the plane electrode (normally grounded). This is known as the point-to-plane or pin-to-plane configuration.

Electrical treeing is normally divided into three stages [4]. First, is the period of incubation when conditions are developed which enable a tree to initiate (inception stage) [6]. No physical damage is visible at this stage and this is the least understood part of the process. It might best be considered as a period during which conditions are developed which enable high energy electrons to be created by the electric field in the

DOI 10.1109/TDEI.2013.003911

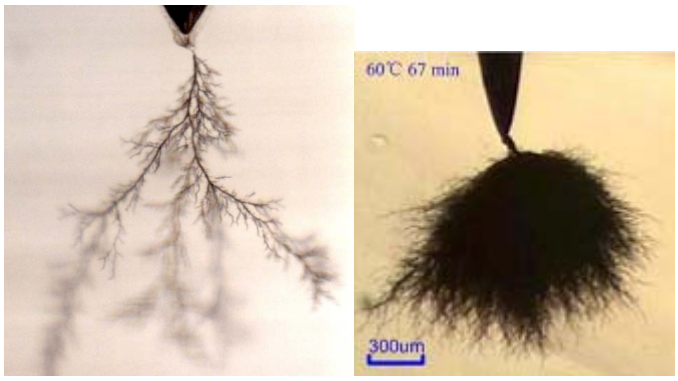

Figure 1. Left: Branch-type electrical tree created in the laboratory [7]. Right: Bush tree [8].

material. Second, the electrical tree grows through electron avalanche (partial discharge) activity resulting in hollow channels of degradation (propagation stage). Third, the tree bridges the insulation (runaway stage). The final breakdown event and its associated destructive current may be considered a further part of the process. During growth, electrical trees can be characterized by different shapes commonly classified for simplicity as: branch (Figure 1 - left), bush (Figure 1 - right) or branch-bush structures (a mix between both) [4]. Electrical trees can have other distinctive shapes or even possess different structures during their evolution [1, 9]. The main methods of electrical tree characterization in the laboratory are: imaging techniques, partial discharge measurements and electroluminescence detection.

One of the first publications containing images of electrical trees was in 1935 where treeing in oil impregnated paper was shown [10]. With the years, failures occurred and pictures from cables containing electrical trees that were in service at normal operating voltage were reported [11, 12]. A historical review of treeing in solid dielectric materials can be found in [5], while a review of experimental work on treeing is presented in [13]. Digital imaging and computers have helped boost the post-processing of data and thus, the possibility of analysis. However, most research and analysis has been focused on two-dimensional images, mainly because of simplicity of acquisition.

This paper reviews techniques previously used for imaging electrical trees and presents the application of X-ray computed tomography for 3-D imaging of electrical trees. Then techniques are compared and evaluated.

2 TECHNIQUES FOR ELECTRICAL TREE IMAGING

There are several microscopy techniques available for the examination of polymers [14, 15]. This section reviews the techniques that have been used to obtain images of electrical trees [16]. These methods can be classified by distinguishing features such as: whether they are destructive, resolution achieved, the nature of the wave applied (e.g. electromagnetic or ultrasound), wavelength of the source applied (e.g. visible light, X-ray, electron beam, laser), among others. Here the techniques are classified as 'optical microscopy', 'electron microscopy' and 'other methods'. A summary of the techniques is presented in Table 1.

2.1 OPTICAL METHODS

The most common imaging technique for electrical trees is 'visible-light microscopy'; see for example Figure 1. Further images using this technique can be seen in [1, 8, 17-22]. The current technology of CCD cameras and microscope systems with digital recording allow analysis of electrical tree growth, making it ideal for analysis as the tree grows, with the possibility of synchronization with partial discharge measurements [23]. The growth of the electrical tree can be readily video recorded [24].

This technique is non-destructive and has been applied to translucent materials such as unfilled epoxy resins, polyethylenes, unfilled silicone rubbers, polypropylene and polyesters. Samples are designed to allow clear 'sight' of the tree. Commercial filled polymers such as silica filled epoxy, clay filled EPDM and ATH filled silicones are unsuitable for this technique because of the associated reduction of transparency.

Much information can be extracted from resulting 2-D optical images of electrical trees as they develop [25]; for example, the shape or structure [1, 9, 18], the fractal dimension [1, 22, 26], the tree length [1, 18, 22], tree growth rate [9] and the ratio of the width and the length of the tree [1].

In practice, the resolution (the closest two points that can be resolved) achieved by optical methods is mainly limited by the transparency of the material and the contrast of the electrical tree with the bulk material. The practical optical resolution is presently around 0.2 μm [14], however, in the application of imaging electrical trees in polymers the resolution achieved is a few micrometers.

A feature of electrical tree growth is that it is associated with partial discharges. These discharges give rise to emission of visible light which can also be detected by microscopy [27-29]. In addition, during inception and later growth, lower but detectable levels of electroluminescence occur [29].

2.2 ELECTRON MICROSCOPY

Electron microscopy can be divided into scanning electron microscopy (SEM) and transmission electron microscopy (TEM) techniques. Both use electrons as a source, but while in SEM the imaging information is obtained by the reflected signals emitted from the surface of a specimen, in TEM the information is obtained by the transmitted electrons that passed through a thin specimen [14].

2.2.1 SCANNING ELECTRON MICROSCOPY (SEM)

In SEM a beam of electrons is focused on the surface of the specimen and scanned along a raster of a parallel contiguous line pattern [30]. The incident beam interacts with the surface of the sample and different signals are emitted as a result of the interaction. These signals, mainly composed of secondary electrons, primary back-scattered electrons and X-rays, are collected to form an image.

Table 1. Techniques for electrical trees imaging.

Technique [1]	Destructive [2]	Advantages (Benefits)	Disadvantages (Limitations)	Information extracted	Resolution [3]	Real time	Example references
Optical	No	Video recording (dynamics of tree growth) More accesible technology (cheaper) More direct visualisation, easier to interpret Possibility of visualizing PD light emissions	Only translucent materials Narrow depth of field	Shape Structure Global dimensions	few (μm) (A) 0.2-0.3 μm (B) [14]	Yes	[1, 8, 17-22, 24]
SEM	Yes	Large depth of field High resolution	Only surface exploration Possible feature damage because the beam Possible modification of the structure when cutting Charging issue	Morphology Micro-structure	tens of (nm) (A) 2-10 nm (B) [14]	No	[31-35]
TEM	Yes	Very high resolution	Complex sample preparation (thin specimen) Possible modification of the feature if etching is used Possible feature damage because the beam	Morphology Micro-structure	> 0.2 nm (B) [14, 36]	No	[33, 37-38, 40]
Ultrasound	No	Non-ionizing, compared e.g. X-ray Comparatively low cost More portable equipment	Immersion in water is normally used Comparatively low resolution Cannot resolve complex structures	Flaw detection	35-50 μm (A) [45, 46]	No	[42, 44, 45]
NMR	No		Very low resolution Comparatively high cost	Affected area	0.7 mm (A) [47]	No	[47, 48]
LSCM	No	Better resolution than conventional optical Possibility of cuasi 3-D view (focusing at diff. depths)	Only translucent materials	As in optical	0.2 μm (A) [51]	No	[50, 51]

[1] Imaging techniques for research purposes, not for diagnosis of equipment insulation.
[2] Destructive means that the feature is irreversibly damaged during the preparation or examination.
[3] (A) Best reported for electrical trees. (B) Capability of the technique or reported for another application.

For sample preparation, the specimen is cut with a microtome typically along a tree branch for exploration of its interior surface [31-34]. Alternatively, cross-sections of the tree can be cut to obtain images of tree holes [35].

This technique is destructive since the sample needs to be microtomed, but it is not dependent on material transparency. The channel-like nature of the trees was demonstrated using this technique [5]. The resolution of SEM systems is less than one nanometer, however, in the case of polymers and electrical trees, the resolution is decreased by problems related to high doses of electrons and low contrast [14].

Another potential problem of using SEM on polymers, is the issue of charging the surface [14]. A method to alleviate this is gold coating the surface [36]. This conductive layer avoids charge accumulation and increases the signal of secondary electrons, improving the signal-to-noise ratio. Another risk is modification of the morphology of the feature under examination by the electron beam or as a result of slicing for sample preparation.

2.2.2 TRANSMISSION ELECTRON MICROSCOPY (TEM)

In TEM a thin specimen is irradiated with an electron beam [36]. Electrons interact with atoms of the bulk of the sample as they pass through it and the image is formed from the transmitted signal. The technique is mainly used to study the morphology of materials. The specimen is sliced into sections, around 100 nm thick, for examination [33, 37], and the sample can be stained to obtain a better contrast [37]. TEM, like SEM, is a destructive method due to the slicing of the sample. Accordingly, it does not require optical transparency of the material. However, the sample preparation is complex since a very thin slice is needed to acquire the 'electron-transparency' of the material. Additionally, samples are normally prepared by permanganic etching process in order to remove surface deformation and etch the microstructures for imaging [38]. The main advantage of this technique is its capability to resolve features below nano-metric size [36, 39]. However, as a rule of thumb, the resolution limit in polymers is about one tenth of the thickness of the specimen [14]. An example of this, is the identification of a tree, immediately after initiation, as a hollow tube of about 50 nm in diameter [40].

2.3 OTHER METHODS

2.3.1 ULTRASOUND

Ultrasound imaging techniques consist of sending ultrasound pulses to an area of interest and capturing the reflected signals coming from the interfaces where differences in acoustic impedance exist. It is a non-destructive method able to detect and characterize flaws in insulation [41-43]. Moreover, this technique has been applied for the detection of electrical trees [42, 44, 45]. In its application, the transducer which sends and receives the ultrasound signals, and the sample are normally immersed into a water tank in order to obtain better transmission avoiding mismatching of acoustic impedances. In [44] the location of an electrical tree was detected close to the surface. That system had an estimated resolution of 50-200 μm. In another example, electrical trees in silicone rubber were detected, but the fine structure of the tree could not be visualized [42]. More recent studies have achieved better resolutions. In [45] branching of a tree could be discriminated with a resolution of around 50 μm. In the application of a proposed modification of the synthetic aperture focusing method, a lateral resolution of around 35 μm is reported [46].

The ultrasound technique requires a compromise between resolution and attenuation: on the one hand, higher frequencies improve resolution, on the other hand, higher frequencies suffer higher attenuation, limiting the accessible depth [42].

In summary, ultrasound techniques are able to detect areas of degradation or treeing, but are unable to resolve the detail and complex structure of electrical trees.

2.3.2 NUCLEAR MAGNETIC RESONANCE

Nuclear magnetic resonance is a spectroscopy which employs radio frequency radiation in magnetic fields to examine properties of the atomic nuclei [47]. It is a non-invasive

technique and does not depend upon the transparency of the material. In attempts to visualize electrical trees using nuclear magnetic resonance, the technique was used to analyze morphological changes in polyethylene. Again, only generally affected areas (areas of treeing) can be detected, rather than any detail, and the reported spatial resolution was around 0.7 mm [47, 48].

2.3.3 LASER SCANNING CONFOCAL MICROSCOPY (LSCM)

In LSCM (or confocal laser scanning microscopy - CLSM) a laser beam is focused into a small area of the sample and scanned to get an image at a certain depth level into the sample. The samples examined are tens of micrometers thick. This technique is considered as the optical equivalent of SEM [49]; moreover, when imaging translucent materials, it has the ability to create 3-D images through the reconstruction of pictures at different depths. This process is called the 'non-invasive serial optical sectioning' [49].

LSCM has been used for imaging water trees [50, 51]. It achieves better resolution than conventional optical microscopy and thicker samples can be examined (200 μm in [50]) than with TEM. The lateral resolution reached using this technique in [51] was around 0.2 μm. This technique has not yet been widely used for scanning insulation materials. Until now, it has been widely used in biomedical imaging [49, 52].

3 THREE- DIMENSIONAL IMAGING

Most of the images of electrical trees available in the literature are in two-dimensions (2-D). This is due to the simplicity of image acquisition. Three-dimensional (3-D) images are required for a more complete representation that does not lose information on the electrical tree structure.

As described in the previous section, laser scanning confocal microscopy has the ability to acquire several 2-D images at different levels of depth, and from them, reconstruct the 3-D view of the feature. However, only a few tens of micrometers in depth can be analyzed and reconstructed; therefore, this method will not be considered as a 3-D imaging technique here. There have been a few attempts of 3-D imaging of electrical trees. One of them was the use of ultrasound [44]. There, a bush-type electrical tree was imaged. However, only a general shape-pattern was obtained and moreover, the technique relied on human recognition of the signals among noise.

Two key methods of construction of 3-D images are now considered: serial sectioning method (SSM) and computed tomography (CT).

Using the SSM [26, 53], the sample is cut in slices with a microtome, and 2-D images taken. The 3-D pattern is reconstructed from the 2-D images. This method is demonstrated for trees in Section 5 using SEM images, where the technique is called "serial block-face SEM" (SBFSEM).

CT images an object from either transmission or reflection data collected by illuminating the object with a penetrating wave from many different angles [54]. In contrast to SSM this is a non-destructive technique. In [53], an optical microscope with a CCD camera was used to take the image of the projected 2-D pattern every 2° from 0° to 180°. However, the reconstructed 3-D pattern did not yield much detail and it was pointed out that the method does not reconstruct a dense bush tree satisfactorily [53], as the details in the interior of the tree are lost.

X-ray tomography has been applied by the authors for 3-D imaging of electrical trees [7]. The description of the technique and the results obtained are presented in the following section.

4 EXPERIMENTAL: X-RAY COMPUTED TOMOGRAPHY (XCT)

4.1 EXPERIMENTAL DETAILS

X-ray computed tomography (XCT) is based on the measurement of transmission of X-rays through the object over a range of angles. A schematic diagram of a typical laboratory micro CT system is shown in Figure 2.

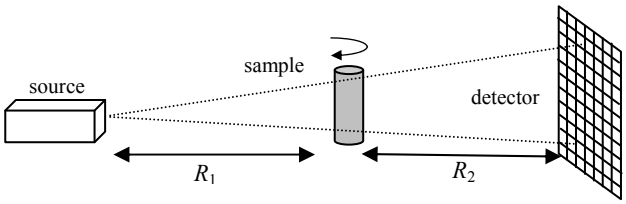

Figure 2. Schematic diagram of a typical laboratory micro CT system having cone-beam geometry.

Recent advances in source and detector technology have enabled resolutions down to one micrometer or less to be routinely achieved with this type of system [55]. Even higher resolutions (down to the tens of nanometer range) can be achieved using X-ray microscopes [55, 56]. These instruments are analogous to visible light microscopes in that the sample is illuminated by X-rays using a condenser optic, and a lens (Fresnel zone plate) is used to focus the X-rays that have passed through the object on to a detector. In this work an Xradia micro-XCT-400 system (Xradia Inc., Pleasanton, CA) was used to provide resolutions down to ~1 μm, while an Xradia nano-XCT-100 microscope was used to provide 150 nm resolution.

For tomography, a series of 2-D radiographs are taken as the sample is rotated about the vertical axis over at least 180°, and these are combined with a reconstruction algorithm to form a virtual 3-D replica of the object [54]. Contrast is typically obtained from the attenuation of X-rays (loss of intensity) as they pass through the object [54]. However, attenuation contrast was poor for the electrical trees at the hard X-ray energies produced by the sources of the two instruments. As an alternative, contrast can be obtained from the shift in the phase of the X-rays as they pass through the object. For the Xradia micro-XCT system the 'in-line' method can be used, in which the phase shift leads to interference fringes being measured on the detector. In the near-Fresnel regime, these fringes act as an edge-enhancement, highlighting sharp boundaries within an object [54, 57]. In

this regime the phase contrast increases with distance between the source and object, and object and detector (R_1 and R_2 respectively in Figure 2) [57]. These distances were optimized for each electrical tree to produce adequate contrast.

For the Xradia nano-XCT microscope, Zernike phase contrast is available, in which the sample is illuminated by a hollow-cone of X-rays, and a phase ring is placed in the back-focal plane of the X-ray lens [56]. The phase ring produces a -3π/2 shift relative to the phase of the X-rays that are undiffracted by the object. However, some of the diffracted rays also pass through the phase ring leading to a 'halo' effect which highlights the boundaries within the object. This effect is manifested in the reconstructed slices as a bright and dark band either side of the boundary as illustrated later.

4.2 IMAGING STUDY CASES

Several point-to-plane samples were prepared. Electrical trees were grown under electrical stress until the desired length of the tree was reached or until electrical breakdown occurred. After the feature was created in the material, the sample was prepared for the X-ray scanning process.

The samples were examined under 2-D X-ray imaging (radiographs) and if they showed no noticeable feature, no tomography was performed. Other cases revealed features under 2-D radiographs. Three of them: an electrical breakdown, a bush-type electrical tree and a branch-type electrical tree, were fully scanned with 3-D XCT technique. Samples 1 and 2 were previously reported [7] and are presented here again with further analysis.

4.2.1 SAMPLE 1: ELECTRICAL BREAKDOWN

A tree was grown in epoxy resin (Huntsman Araldite® LY5052 - Aradur® HY5052, a cold curing epoxy system), until a breakdown channel occurred. Details concerning the sample preparation and breakdown are given in [7]. For scanning, the sample was cut down to a 3 mm diameter cylinder containing the breakdown feature to get better contrast and resolution. It was observed that the sample had changed to a darker color during the exposure to X-ray (the scan time was ~14 h and 2001 radiographs were taken over 188°). However, no changes in the structure of the electrical tree were evident when comparing the radiographs taken at the start and end of the scan. After reconstruction, the final voxel (volumetric pixel) size was 2.4 µm. Features smaller than this size cannot be fully resolved and thus, could not be analyzed. Avizo image processing software (VSG, Burlington MA) was then used to segment the breakdown feature.

4.2.2 SAMPLE 2: BUSH-TYPE ELECTRICAL TREE

An electrical tree was created using a similar procedure as for Sample 1; however in this case, a more optically transparent polymer was used (Norland® Optical Adhesive 61, a colorless photopolymer). Details about the sample preparation and electrical tree creation are given in [7]. The tree created was a bush-type electrical tree of around 1.2 mm wide and 0.8 mm long (a video of the electrical tree growth can be seen in [24]). To get better contrast in the scan, the sample cylinder diameter was decreased to 2 mm. The specimen was scanned at higher magnification than for Sample 1 for 54 h during which time 361 radiographs were taken over 182°. In this case, no color change was noticeable in the sample. The reconstruction of the tree resulted in a voxel size of 1 µm and Avizo software was used to segment the electrical tree.

4.2.3 SAMPLE 3: BRANCH-TYPE ELECTRICAL TREE

The sample consisted of an epoxy resin cube of the same material and dimensions as Sample 1, with an acupuncture needle (Hwato® 0.35 mm, ~5 µm tip radius) inserted leaving a 2 mm gap between the needle tip and the bottom of the cube. The sample was stressed under 10 kVrms 50 Hz until the electrical tree was noticeable optically. The resulting feature was a branch-type electrical tree of around 200 µm length. For XCT, the sample was machined to a cylinder of around 2 mm diameter and scanned for 60 h using the Xradia nano-XCT microscope at 150 nm resolution, during which time 721 radiographs were taken over 180º. Limitations in the accuracy of the instrument rotation stage meant that the sample was subjected to random movement ('wobble') as it is rotated. This wobble was corrected for by tracking the tip of the needle through the series of radiographs using image correlation and then aligning the radiographs prior to reconstruction. The field of view was around 60 µm, meaning that only around a third of the tree length was imaged. After the scan, a localized change in color of the sample was observed. Again there were no noticeable differences in the tree structure when comparing the radiograph taken at 0° at the start of the scan and at 180° close to the end of the scan. The voxel size of the reconstruction was 0.13 µm. Again, Avizo software was used to segment and create the 3-D model of the electrical tree.

4.3 RESULTS

4.3.1 SAMPLE 1: ELECTRICAL BREAKDOWN

The electrical breakdown and its reconstruction are shown in Figure 3. An animation with a 3-D rotation of the breakdown channel is available [24]. The breakdown tube was

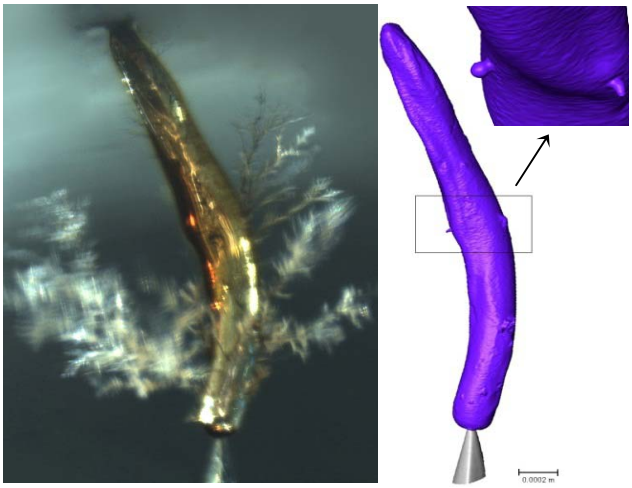

Figure 3. Sample1 - Electrical breakdown. Left: Optical microscopy. Right: 3-D X-ray tomography. Scale bar: 200 µm [7].

fully revealed by the technique, and some of the thicker tree branches projecting from the tube were captured.

After segmenting the tube, the following measurements were determined using Avizo: volume 0.073 mm^3, mean diameter 180 µm and length along the center path 2.46 mm.

The fine structures of the electrical tree were not captured; however, some protuberances in the breakdown channel were evident marking the presence of the branches of the remaining tree. The reason why tree branches were not revealed, but the breakdown channel was, may not be only because they were smaller than the breakdown tube, but also because the breakdown channel was composed of carbonized material (due to the high temperature breakdown event) which may help in obtaining a better contrast between the bulk dielectric and the feature.

4.3.2 SAMPLE 2: BUSH-TYPE ELECTRICAL TREE

The reconstruction results using XCT for Sample 2 are shown in Figure 4 and Figure 5. The very fine tips of the electrical tree were not clearly distinguishable due to noise in the data, and could not be segmented for further quantitative analysis. Only ~600 µm of tree length is presented here. A virtual animation with axial rotation of the reconstructed electrical tree is shown in [24].

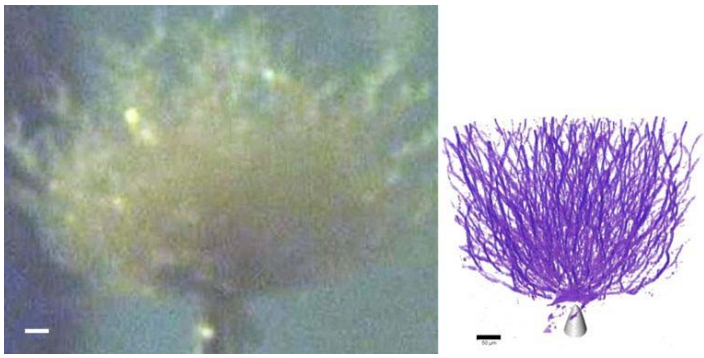

Figure 4. Sample 2 - Bush-type electrical tree. Left: Optical camera. Right: 3-D rendering of the XCT reconstruction. Scale bar: 50 µm [7].

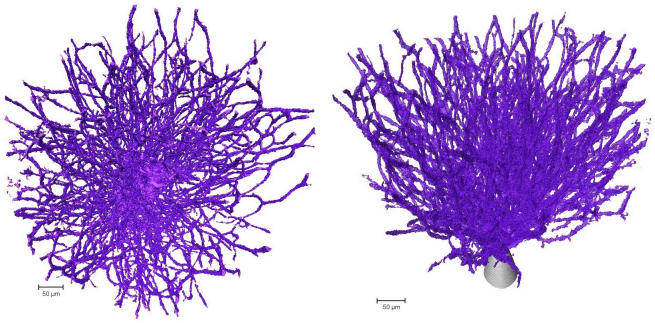

Figure 5. X-ray reconstruction Sample 2. Left: view from the top. Right: another view-angle. Scale bar: 50 µm.

Volumetric measurements were taken using Avizo software. The volume of the tree was 1.78×10^6 μm^3, while the volume enclosing all points in the tree was calculating using the convex hull to be 5.06×10^7 μm^3. The convex hull is the smallest convex polyhedral surface that contains the entire feature. Accordingly, the proportion of tree volume degraded of Sample 2 was 3.5% (ratio between volume and convex hull volume of the tree). The mean diameter of the channels was calculated to be 4.4 µm (with a standard deviation of 1.7 µm) using the local thickness plugin for ImageJ software.

As an additional method of characterizing the tree, the calculation of the tortuosity of the branches of the tree was explored. The simplest method of calculating tortuosity is the ratio between the length along the route through the tree and the Euclidean distance from the starting point to the end point. The tortuosity was calculated by first applying the medial axis transform [58] which determines the center-line along all branches in the tree. Shortest paths through the tree were then generated from a single starting point, this being the closest point to the tip of the needle, to the end point of each of the branches. The shortest paths were determined using Dijkstra's algorithm [59]. The tortuosity of each path was then calculated using the method presented in [60], which involves sampling the path on a scale related to the local thickness of the channel. This method minimizes the effect of noise in the segmentation which can lead to the center-lines having an erroneous high-spatial frequency component, leading to an overestimation of the tortuosity. In the case of Sample 2, the mean tortuosity over all paths was 1.6 with a standard deviation of 0.6.

The change in the tree with distance from the needle was investigated by considering cross-sections/slices through the data, which were aligned approximately perpendicular to the major axis of the needle and tree. Cross-sections at different distances from the needle tip are shown in Figure 6. An animation of the cross-sections (slices) along the progression of the tree can be seen in [24].

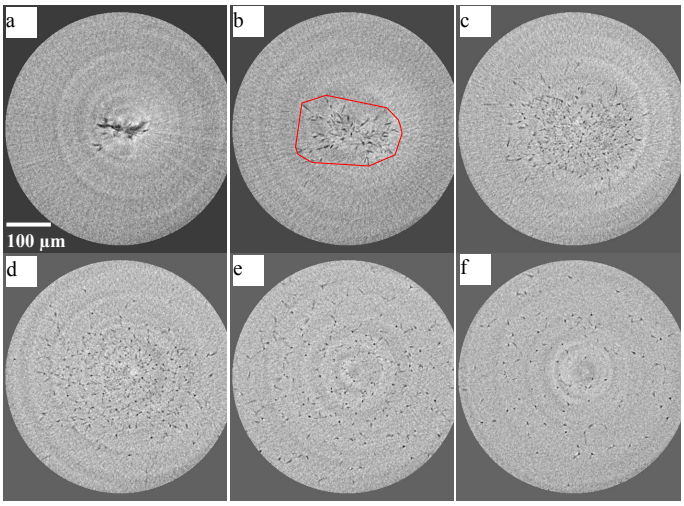

Figure 6. Cross-sections of the reconstructed electrical tree, Sample 2. Distances from the tip in µm: a. 20, b. 50, c. 100, d. 150, e. 250, f. 350 [7].

The number of electrical tree channels as a function of the distance from the needle tip is shown in Figure 7 (top, continuous line), which characterizes the bifurcation through the tree. The total channel area and the 2-D convex hull area (are enclosing all the channels) in each cross-section are represented as a function of distance from the needle tip in Figure 7 (bottom). The area of the 2-D convex hull on each slice was determined using Matlab 2012a (Mathworks Inc, Natick, MA) (see polygon enclosing the entire set of tree

channels in Figure 6b). The proportion of area degraded is defined as the ratio between the total channel area and the convex hull area is represented in Figure 7 (top, dashed line).

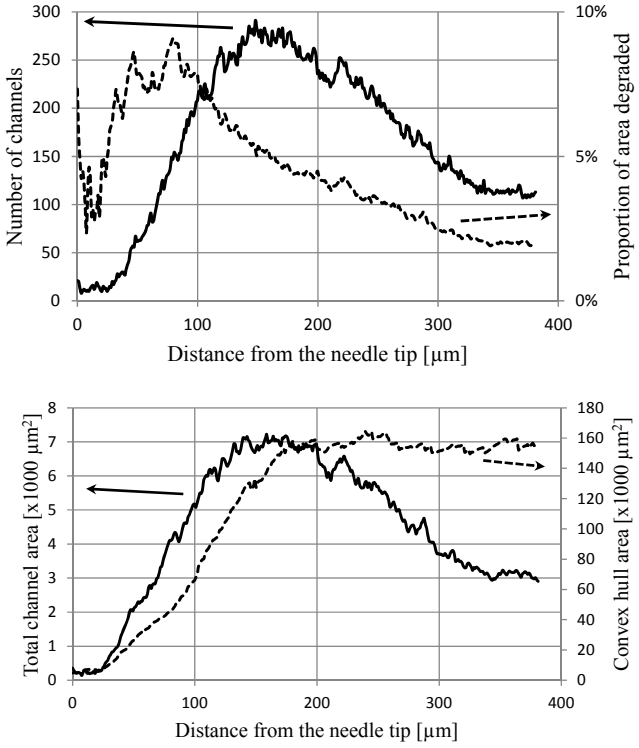

Figure 7. Cross-section analysis of Sample 2. Top: Continuous line, number of electrical tree channels. Dashed line, proportion of area degraded. Bottom: Continuous line, total cross-sectional area covered by tree channels. Dashed line, convex hull cross-sectional area of tree channels [7].

The graphs of Figure 7 show that the change of the number of branches and area covered by the channels is in accordance with the visible aspect of the bush-type tree. By 200 µm from the tip, the tree covered a larger cross-sectional area than the field of view. At this point, the convex-hull area becomes artificially constant, while the number of channels and the total channel area decrease as the tree becomes less dense.

In the case of Sample 2, the X-ray technique was able to reveal the fine channels of the electrical tree which was not the case of Sample 1, where only the breakdown tube was observed. This difference is partly due to a higher magnification being used when scanning Sample 2. However, there are other possible reasons including that the tree-channels in Sample 2 could have been considerably thicker than in Sample 1 (so that sub-micron resolution would be required for Sample 1). The samples were made of different materials, so that the nature of the channels (in particular the material in the channel and the channel surfaces) in Sample 2 might allow better contrast for X-ray imaging than in Sample 1. Overall, the results suggest that it is necessary to have a voxel resolution of less than ~2 µm in order to successfully image the majority of features in the electrical trees with X-ray tomography. However, much higher resolutions are likely to be needed when studying early-stage tree development. The applicability of using X-ray nano-tomography is therefore explored for Sample 3 in the following section.

4.3.3 SAMPLE 3: BRANCH-TYPE ELECTRICAL TREE

A 3-D rendering of the branch-type tree is shown in Figure 8 (with the needle omitted) with an accompanying animation available at [24]. A volume of 59 µm x 66.6 µm x 64.6 µm was imaged with a voxel size of 0.13 µm. It was necessary to image at the tip of the needle, as this feature was used to align the radiographs (i.e. correct for stage wobble) prior to reconstruction (see Section 4.2.3). Therefore, the actual distance along tree in the direction of the needle available for analysis was 42.1 µm (325 slices). No optical image is provided here since a good quality image was not achievable in this case.

To improve signal-noise-ratio of the reconstructed slices, a uni-directional bilateral filter was applied, this being a variation of the standard bilateral filter developed by [61]. A new intensity was calculated for each voxel, by considering the intensity of those voxels within 20 slices directly above and below the current voxel (the vertical direction being the primary axis of the tree). The intensities of these voxels were averaged using a Gaussian weighting related to the difference in intensity to that of the current voxel.

The channels in the tree were segmented using a grey-level threshold to select the dark band around the inner edges of the channels produced by the halo artifact (see Section 4.1). In a small number of places, the magnitude of the halo artifact was reduced and a limited amount of manual segmentation was required. A hole-filling algorithm was then applied in Avizo to select all voxels bounded by the dark bands, and hence segment the full internal volumes of the channels. However, it was noticed that some branches appeared to be disconnected from the main tree. This can arise if parts of the channels have a diameter less than a few voxels across or have low contrast, which in both cases means that the channel section cannot be distinguished above the noise level. These disconnected branches were considered for the measurements presented below, except in the case of tortuosity, since they do not share the same starting point as the other branches.

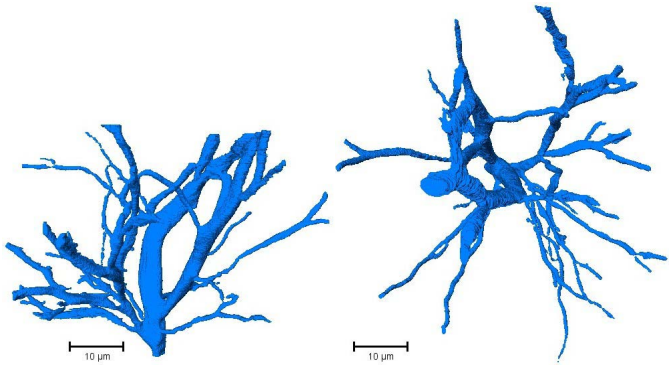

Figure 8. Sample 3. Branch-type electrical tree. Left: Front view. Right: Top view. Scale bar: 10 µm.

The tree volume and convex hull volume were 1.30×10^3 µm^3 and 6.98×10^4 µm^3, respectively (calculations made using Avizo software). Thereby, the proportion of volume degraded was 1.9%. The shortest paths from the needle to each branch end-point were less convoluted compared to the bush-type tree (Sample 2), with the mean tortuosity being 1.25 (with a standard deviation of 0.09), using the procedure described for

Sample 2 in Section 4.3.2. There are, however, far fewer branches in this data set.

Six cross-sectional slices are shown in Figure 9 with an accompanying animation showing all slices available to view in [24]. These images demonstrate the 'halo' effect which highlights the boundaries within the object as discussed in Section 4.1.

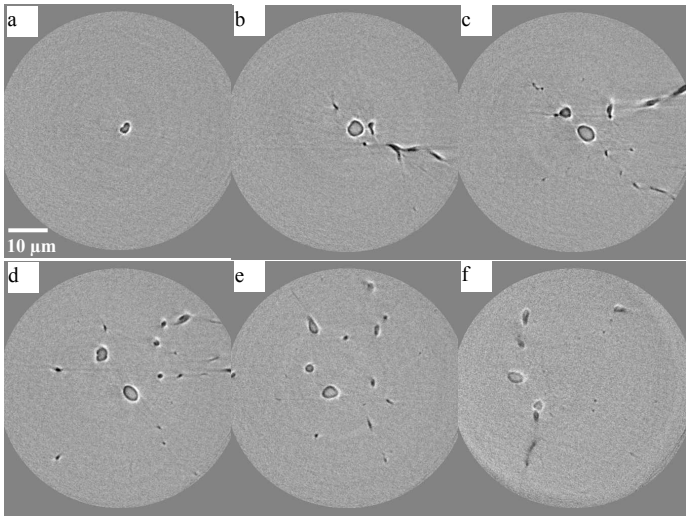

Figure 9. Cross-sections of the Sample 3. Distances from the starting point of the tree in µm: a. 0, b. 7, c. 14, d. 21, e. 31, f. 42.

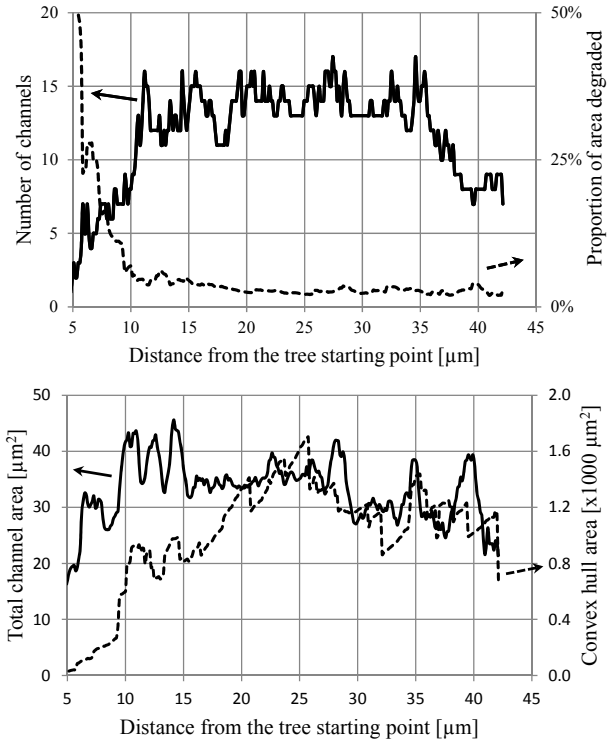

Figure 10. Cross-section analysis of Sample 3. Top: Continuous line, number of electrical tree channels. Dashed line, proportion of area degraded.
Bottom: Continuous line, total cross-sectional area covered by tree channels. Dashed line, convex hull cross-sectional area of tree channels.

The mean diameter of the channels was determined to be 1.9 µm (with a standard deviation of 1 µm), calculated as before with ImageJ software. The number of tree channels as a function of the distance from the starting point of the tree is shown in Figure 10 (top, continuous curve). Additionally, the total area and the convex hull area of the tree channels are shown in Figure 10 (bottom); and the proportion of area degraded (ratio between total area and convex hull area of the tree channels) is shown in Figure 10 (top, dashed curve). The values are shown from 5 µm to obtain better resolution in the plot, due to the fact that near to the tree starting point there was only one tree channel, yielding to a proportion of area degraded close to 100%.

4.4 COMPARISON OF SAMPLES 2 AND 3

It is necessary to consider that Sample 2 and Sample 3 were made of different materials, and moreover, Sample 2 was stressed much longer than Sample 3, resulting in a larger and more mature tree. Thus, it was necessary to scan the bush-type (Sample 2) and branch-type (Sample 3) electrical trees, with different instruments, having considerably different fields of view. Therefore, direct comparison between the measurements made for the two trees is difficult. Nevertheless, the global parameters (those calculated using the whole data) are indicative of differences in the structure of the trees. For example, the mean channel diameter confirms that it was necessary to scan the branch-type tree at a higher resolution. In addition, particular local properties measured at the same distance from the needle tip (Sample 2) or starting point of the tree (Sample 3) directly relate to differences in tree structure.

The local properties were measured on a slice that was 35 µm distant from the needle tip (Sample 2) or the starting point of the tree (Sample 3). The comparison of these calculated parameters is shown in Table 2. For the specific meaning of the parameters and the calculation method, refer to the previous sections.

Table 2. Comparison of some parameters of Sample 2 and Sample 3.

	Sample 2 (bush tree)	**Sample 3** (branch tree)
Global parameters [1]		
Mean diameter	4.4 µm	1.9 µm
Standard deviation	1.7 µm	1.0 µm
Tortuosity	1.6	1.25
Standard deviation	0.6	0.09
Proportion of volume degraded [2]	3.5%	1.9%
Local parameters at 35 µm [3]		
Number of channels	27	14
Proportion of area degraded [2]	6.8%	2.7%
Channels area	941 μm^2	38 μm^2
Degraded volume [4]	93021 μm^3	1085 μm^3

[1] The entire electrical tree is considered.
[2] Ratio between volume (area) and convex hull volume (area).
[3] Only the cross-section slice located at 35 µm is considered.
[4] Accumulated volume of the electrical tree from 0 to 35 µm.

5 EXPERIMENTAL: SERIAL BLOCK-FACE SEM

Serial block-face scanning electron microscopy (SBFSEM) was deployed as an alternative for 3-D imaging of electrical trees [62]. After XCT, Sample 2 was examined using an SEM microtomy procedure which consists of slicing the sample and

imaging its surface [63]. A Gatan 3View® system was used to perform the automated sectioning process. The 3View® was housed within an FEI Quanta FEG 250 instrument, which has a field emission gun and a variable pressure chamber. The microscope was operated at low vacuum using water vapor to reduce problems with sample charging. The accelerating voltage was set to 10 kV and the pressure 120 Pa.

The 3-D reconstruction of the final portion (255 μm thickness) of the tree in Sample 2 is presented in Figure 11. A total of 1273 SEM images were taken from cross-sections of the tree, with a cut thickness of 0.2 μm. The dimensions of each image were 4000 px by 4000 px with a pixel size of 0.2 μm. The 3-D reconstruction was completed using Avizo software, after brightness correction and noise filtering of the original images.

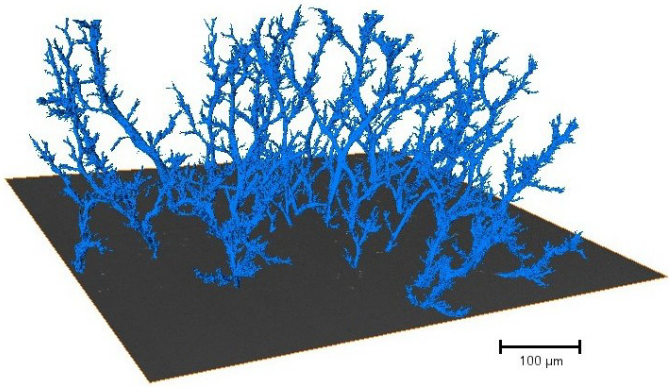

Figure 11. 3-D imaging of the final portion of Sample 2 using SBFSEM.

6 DISCUSSION

Three-dimensional imaging of electrical trees through XCT is a non-destructive and high resolution technique, which has provided promising results in the characterization of the structure of the trees. In practice, the absorption contrast between the bulk material and the electrical tree structure (which is likely to be composed of air/gas voids and/or degraded material) was found to be insufficient to reveal the electrical tree. The successful imaging of electrical trees presented here was achieved with the phase contrast enhancement available on the XCT systems used.

A color change was observed during the X-ray exposure in the case of epoxy resin, indicating that the X-ray beam produced chemical ageing in the material. However, no significant modification occurred in the electrical tree structure, since no visible difference was evident when comparing the radiographs taken at the start and end of the scan, indicating that the color change should not affect the imaging results. This change in color was not observed in the transparent material, suggesting that this material is more suitable for X-ray imaging.

Computed tomography enables quantification of the electrical tree in 3-D. In the cases studied, not only did the virtual replicas enable the surface and internal details of the electrical tree to be observed at any given angle, but also enabled a wide range of measurements to be taken to characterize and compare the different samples. New indices were developed to analyze both 3-D features as well as 2-D features on any given virtually slice through the sample. Thus, a more complete insight can be achieved. The entire electrical tree can be assessed by extracting for example the mean diameter and tortuosities of the channels. Moreover, the progression of the tree away from its initiation point is measurable using the 2-D virtual slices, as characterized by indices such as the number of channels and channels area, among others.

For example, the degraded volume from the starting point of the tree to 35 μm was 93,021 μm^3 and 1085 μm^3, for Sample 2 and 3 respectively. This notable difference is in concordance with the visual aspect and the expected difference between a branch and a bush-type electrical tree. However, this difference is not prominent when comparing the proportion of volume degraded of the entire electrical tree (3.5% for Sample 2 – bush-tree and 1.9% for Sample 3 – branch-tree). Though the volume degraded in Sample 3 is much larger than in Sample 3 (1.78×10^6 μm^3 vs. 1.30×10^3 μm^3), the convex hull volume that encloses the tree is also much larger (5.06×10^7 μm^3 vs. 6.98×10^4 μm^3), resulting in relatively similar values for the proportion of volume degraded. Analyzing the cross-section that was located 35 μm from the starting point of the tree, the area covered by the tree channels for Sample 2 and 3 were 941 μm^2 and 38 μm^2 respectively. Accordingly, the number of channels in Sample 2 was almost the double that in Sample 3 (27 and 14 respectively). Comparing the entire electrical tree, also worth noting was the difference in the mean diameter of tree channels. For Sample 2 was 4.4 μm and for Sample 3 was 1.9 μm. This may be due to the difference in material, but also, mainly because Sample 2 was stressed much longer than Sample 3, giving more chances to partial discharge erosion of the tree channel walls, thus increasing their diameter.

These parameters certainly add valuable information into the analysis of degradation through electrical trees in polymeric insulation. However, more data is needed to establish the range that these parameters typically take and hence determine criteria by which the tree structure can be interpreted, as compared to established conventional parameters such as fractal dimension. In this study the feasibility of creating similar images generated by the destructive SBFSEM method, has shown that this too can be used to generate an equivalent data set.

In some cases of the application of XCT, the electrical tree was not seen. It is not clear why some electrical trees are visualized and not others. It might an issue of resolution (very fine tree channels) and also, it might be related to the particular treeing situation (surface chemistry of the channels) in the material that provides better X-ray contrast between the feature and the bulk material.

7 CONCLUSION

It has been shown here that unique insight into the structure of electrical trees can be achieved by generating a 3-D replica using the XCT imaging technique with phase contrast enhancement. In one case presented using the nano-XCT system, features below one-micrometer could readily be seen. In addition, serial block-face scanning electron microscopy

(SBFSEM) was deployed. Whilst being destructive, this too showed promise as a technique for creating 3-D replica.

It has been established that for all trees absorption contrast was not sufficient at the hard X-ray energies produced by typical laboratory X-ray sources. Phase contrast was required to take advantage of the more sensitive shift in the phase of the X-rays as they propagate through low atomic number/low density materials such as epoxy resin.

Tools have been presented that can be used to quantify the 3-D reconstructed model and distinguish between the distinctive shapes of the different types of trees. Characteristics can be extracted from the model, such as the diameter and tortuosity of tree channels, as well as the overall tree volume and net density of damage. The capability of taking virtual slices through the replica brings the possibility of exploring inside the electrical tree without the destruction of the specimen.

The use of XCT and SBFSEM for imaging electrical trees have been shown to provide techniques to create 3-D virtual replicas of trees through which new valuable information can be extracted. These tools are expected to enable a deeper understanding of electrical treeing phenomenon.

ACKNOWLEDGMENT

Roger Schurch would like to thank the Dielectrics and Electrical Insulation Society (IEEE-DEIS) for the Graduate Fellowship Award which was used to fund this work. R. S. also wishes to acknowledge the scholarship support of CONICYT-Chile (Chilean Research Council). Philip Withers would like to acknowledge funding from EPSRC for the Manchester X-ray Imaging Facility under EP/F007906/1 and EP/F028431/1. The authors thank Dr. Tobias Starborg in the EM facility at the Faculty of Life Sciences in the University of Manchester for his assistance, and the Wellcome Trust for equipment grant support to the EM facility.

REFERENCES

[1] Z. Xiaoquan and G. Chen, "Propagation mechanism of electrical tree in XLPE cable insulation by investigating a double electrical tree structure," IEEE Trans. Dielectr. Electr. Insul., Vol. 15, pp. 800-807, 2008.

[2] N. H. Malik, A. A. Al-Arainy, and M. I. Qureshi, *Electrical Insulation in Power Systems*. New York: Marcel Dekker, Inc., 1998.

[3] S. J. Dodd, "A deterministic model for the growth of non-conducting electrical tree structures," J. Phys. D: Appl. Phys., Vol. 36, pp. 129-141, 2003.

[4] L. A. Dissado and J. C. Fothergill, *Electrical Degradation and Breakdown in Polymers,* London, UK, Peter Peregrinus Ltd., 1992.

[5] R. M. Eichhorn, *"Treeing in Solid Organic Dielectric Materials",* Chapter 4 in *Engineering Dielectrics,* Editors, R. Bartnikas and R. M. Eichhorn, Vol. 2A. Philadelphia, USA, ASTM, 1983.

[6] N. Shimizu and C. Laurent, "Electrical tree initiation," IEEE Trans. Dielectr. Electr. Insul., Vol. 5, pp. 651-659, 1998.

[7] R. Schurch, S. M. Rowland, R. S. Bradley, and P. J. Withers, "A novel approach for imaging of electrical trees," IEEE Conf. Electr. Insul. Dielectr. Phenomena (CEIDP), pp. 593-596, 2012.

[8] B. X. Du, Z. L. Ma, Y. Gao, and T. Han, "Effect of ambient temperature on electrical treeing characteristics in silicone rubber," IEEE Trans. Dielectr. Electr. Insul., Vol. 18, pp. 401-407, 2011.

[9] M. Bao, X. Yin, and J. He, "Structure characteristics of electrical treeing in XLPE insulation under high frequencies," Physica B: Condensed Matter, Vol. 406, pp. 2885-2890, 2011.

[10] D. M. Robinson, "The breakdown mechanism of impregnated paper cables," J. Inst. Electrical Engineers, Vol. 77, p. 90, 1935.

[11] W. Vahlstrom, "Investigation of Insulation Deterioration in 15 KV and 22 KV Polyethylene Cables Removed from Service," IEEE Trans. Power App. Syst., Vol. 91, pp. 1023-1035, 1972.

[12] J. H. Lawson and W. Vahlstrom, "Investigation of Insulation Deterioration in 15 KV and 22 KV Polyethylene Cables Removed from Service - Part II," IEEE Trans. Power App. Syst., Vol. 92, pp. 824-835, 1973.

[13] E. J. McMahon, "A Tutorial on Treeing," IEEE Trans. Electr. Insul., Vol.13, pp. 277-288, 1978.

[14] G. H. Michler, *Electron microscopy of polymers*, Springer, 2008.

[15] J. C. Fothergill, G. C. Montanari, G. C. Stevens, C. Laurent, G. Teyssedre, L. A. Dissado, U. H. Nilsson, and G. Platbrood, "Electrical, microstructural, physical and chemical characterization of HV XLPE cable peelings for an electrical aging diagnostic data base," IEEE Trans. Dielectr. Electr. Insul., Vol. 10, pp. 514-527, 2003.

[16] R. Schurch, S. M. Rowland, and P. J. Withers, "Techniques for electrical tree imaging," IEEE Int'l. Conf. Imaging Systems and Techniques (IST), pp. 409-414, 2012.

[17] A. S. Vaughan, S. J. Dodd, and S. J. Sutton, "A Raman microprobe study of electrical treeing in polyethylene," J. Materials Science, Vol. 39, pp. 181-191, 2004.

[18] C. Xiangrong, X. Yang, C. Xiaolong, S. J. Dodd, and L. A. Dissado, "Effect of tree channel conductivity on electrical tree shape and breakdown in XLPE cable insulation samples," IEEE Trans. Dielectr. Electr. Insul., Vol. 18, pp. 847-860, 2011.

[19] G. Chen and C. Tham, "Electrical treeing characteristics in XLPE power cable insulation in frequency range between 20 and 500 Hz," IEEE Trans. Dielectr. Electr. Insul., Vol. 16, pp. 179-188, 2009.

[20] S. Bahadoorsingh and S. M. Rowland, "Investigating the influence of the lubricant coating on hypodermic needles on electrical tree characteristics in epoxy resin," IEEE Trans. Dielectr. Electr. Insul., Vol. Vol. 17, pp. 701-708, 2010.

[21] S. Bahadoorsingh, R. Giussani, and S. M. Rowland, "The influence of interfaces and channels on electrical tree growth in epoxy resin," IEEE Conf. Electr. Insul. Dielectr. Phenomena (CEIDP), pp. 1-4, 2010.

[22] A. Xie, X. Zheng, S. Li, and G. Chen, "Investigations of electrical trees in the inner layer of XLPE cable insulation using computer-aided image recording monitoring," IEEE Trans. Dielectr. Electr. Insul., Vol. 17, pp. 685-693, 2010.

[23] N. Hozumi, T. Okamoto, and H. Fukagawa, "Simultaneous Measurement of Microscopic Image and Discharge Pulses at the moment of Electrical Tree Initiation," Jap. J. App.Phys., Vol. 27, pp. 572-576, 1988.

[24] R. Schurch, S. M. Rowland, R. S. Bradley, and P. J. Withers, "Electrical Trees", CEIDP, 2013. Available: http://www.youtube.com/user/ElectricalTreesCEIDP/videos

[25] S. Bahadoorsingh, R. Balliram, C. Sharma, and S. M. Rowland, "Development of a software tool to evaluate electrical tree growth images," IEEE Conf. Electr. Insul. Dielectr. Phenomena (CEIDP), pp. 768-771, 2011.

[26] K. Kudo, "Fractal analysis of electrical trees," IEEE Trans. Dielectr. Electr. Insul., Vol. 5, pp. 713-727, 1998.

[27] C. Laurent and C. Mayoux, "Analysis of the Propagation of Electrical Treeing Using Optical and Electrical Methods," IEEE Trans. Electr. Insul., Vol. 15, pp. 33-42, 1980.

[28] S. J. Dodd, N. M. Chalashkanov, and J. C. Fothergill, "Partial discharge patterns in conducting and non-conducting electrical trees," IEEE Int'l. Conf. Solid Dielectr. (ICSD), pp. 1-4, 2010.

[29] S. S. Bamji, "Electroluminescence-a technique to detect the initiation of degradation in polymeric insulation," IEEE Electr. Insul. Mag., Vol. 15, No. 3, pp. 9-14, 1999.

[30] A. Bogner, P. H. Jouneau, G. Thollet, D. Basset, and C. Gauthier, "A history of scanning electron microscopy developments: Towards "wet-STEM imaging," Micron, Vol. 38, pp. 390-401, 2007.

[31] S. Alapati and M. J. Thomas, "Influence of nano-fillers on electrical treeing in epoxy insulation," IET Sci., Measurement Techn., IET, Vol. 6, pp. 21-28, 2012.

[32] J. Wu, T. Iizuka, K. Monden, and T. Tanaka, "Characteristics of initial trees of 30 to 60 um length in epoxy/silica nanocomposite," IEEE Trans. Dielectr. Electr. Insul., Vol. 19, pp. 312-320, 2012.

[33] T. Iizuka, Y. Ohki, and T. Tanaka, "Effects of coupling agent and filler dispersion on V-t characteristics of epoxy/silica nanocomposites," IEEE Int'l. Symp. Electr. Insul. Materials (ISEIM), pp. 60-63, 2008.

[34] A. S. Vaughan, I. L. Hosier, S. J. Dodd, and S. J. Sutton, "On the structure and chemistry of electrical trees in polyethylene," J. Phys. D: App. Phys., Vol. 39, p. 962, 2006.
[35] C. Yu, T. Imai, Y. Ohki, and T. Tanaka, "Tree initiation time evaluation of epoxy/silica composites by partial discharge detection," IEEE Int'l. Conf. Prop. Applic. Dielectr. Materials (ICPADM), pp. 404-407, 2009.
[36] L. Reimer and H. Kohl, *Transmission Electron Microscopy: Physics of ImageFformation*, Springer, 2008.
[37] N. Hozumi, M. Ishida, T. Okamoto, and H. Fukagawa, "The influence of morphology on electrical tree initiation in polyethylene under AC and impulse voltages," IEEE Trans. Electr. Insul., Vol. 25, pp. 707-714, 1990.
[38] L. Markey and G. C. Stevens, "Microstructural characterization of XLPE electrical insulation in power cables: determination of void size distributions using TEM," J. Phys. D: App. Phys., Vol. 36, pp. 2569-2583, 2003.
[39] D. B. Williams and C. B. Carter, *Transmission Electron Microscopy: a Textbook for Materials Science*, Springer, 2009.
[40] N. Hozumi, T. Okamoto, and H. Fukagawa, "TEM observation of electrical tree paths and micro-structures in polyethylene," IEEE Int'l. Symp. Electr. Insul., pp. 331-334, 1988.
[41] D. W. Auckland, A. J. McGrail, C. D. Smith, B. R. Varlow, J. Zhao, and D. Zhu, "Application of ultrasound to the inspection of insulation," IEE Proc. Science, Meas. and Techn., Vol. 143, pp. 177-181, 1996.
[42] H. Ueno, P. Walter, C. Cornelissen, and A. Schnettler, "Resolution evaluation of ultrasonic diagnosis tools for electrical insulation devices and the detection of electrical trees," IEEE Trans. Dielectr. Electr. Insul., Vol. 14, pp. 249-256, 2007.
[43] G. Thomas, D. Flores-Tapia, S. Pistorius, and N. Fernando, "Synthetic aperture ultrasound imaging of XLPE insulation of underground power cables," IEEE Electr. Insul. Mag., Vol. 26, No. 3, pp. 24-34, 2010.
[44] E. Watanabe, T. Moriya, and M. Yoshizawa, "Ultrasonic visualization method of electrical trees formed in organic insulating materials," IEEE Trans. Dielectr. Electr. Insul., Vol. 5, pp. 767-773, 1998.
[45] S. Kida, Y. Murakami, M. Nagao, and N. Hozumi, "Visualization of electrical trees by 80 MHz-band pulsed ultrasound," IEEJ Trans. Fundamentals and Materials, Vol. 131, pp. 792-796, 2011.
[46] J. J. M. Chan, J. R. B. Taylor, and G. Thomas, "Ultrasound high resolution imaging using a modified synthetic aperture focusing method," IEEE Int'l. Conf. Imaging Systems and Techniques (IST), pp. 611-615, 2012.
[47] F. Weigand, H. W. Spiess, B. Blumich, G. Salge, and K. Moller, "Nuclear magnetic resonance imaging of electrical trees in PE," IEEE Trans. Dielectr. Electr. Insul., Vol. 4, pp. 280-285, 1997.
[48] P. Blumler, N. Paus, and G. Salge, "Nuclear magnetic resonance imaging of morphological changes during electrical treeing in polyethylene due to partial discharges," IEEE Int'l. Conf. Conduction and Breakdown Solid Dielectr. (ICSD), pp. 168-172, 1998.
[49] D. M. Shotton, "Confocal scanning optical microscopy and its applications for biological specimens," J. Cell Science, Vol. 94, pp. 175-206, 1989.
[50] S. Haridoss, D. M. Shinozaki, and P. C. Cheng, "Laser scanning confocal light microscopy of cable materials," IEEE Int'l. Symp. Electr. Insul., pp. 392-397, 1990.
[51] E. Moreau, C. Mayoux, C. Laurent, and A. Boudet, "The structural characteristics of water trees in power cables and laboratory specimens," IEEE Trans. Electr. Insul., Vol. 28, pp. 54-64, 1993.
[52] S. W. Paddock, "Confocal laser scanning microscopy," Biotechniques, Vol. 27, pp. 992-1004, 1999.
[53] H. Uehara and K. Kudo, "The 3-D fractal analysis of electrical trees using a serial sectioning method and a CT method," IEEE Int'l. Conf. Conduction and Breakdown Solid Dielectr. (ICSD), pp. 309-312, 1998.
[54] A. C. Kak and M. Slaney, *Principles of Computerized Tomographic Imaging*, Society for Industrial and Applied Mathematics, 2001.
[55] P. J. Withers, "X-ray nanotomography," Materials Today, Vol. 10, pp. 26-34, 2007.
[56] M. Feser, J. Gelb, H. Chang, H. Cui, F. Duewer, S. H. Lau, A. Tkachuk, and W. Yun, "Sub-micron resolution CT for failure analysis and process development," Meas. Sci. Technol., Vol. 19, 094001, 2008.
[57] R. S. Bradley, A. McNeil, and P. J. Withers, "An examination of phase retrieval algorithms as applied to phase contrast tomography using laboratory sources," Proc. SPIE, Developments in X Ray Tomography, San Diego, California, USA, pp. 780404-10, 2010.
[58] R. Katz and S. Pizer, "Untangling the Blum Medial Axis Transform," Int'l. J. Comp. Vision, Vol. 55, pp. 139-153, 2003.
[59] E. W. Dijkstra, "A note on two problems in connexion with graphs," Numerische Mathematik, Vol. 1, pp. 269-271, 1959.
[60] R. S. Bradley and J. P. Withers, "Measurement of tortuosity of 3D tube-like structures with surface texture from volumetric image data," in preparation.
[61] C. Tomasi and R. Manduchi, "Bilateral filtering for gray and color images," Int'l. Conf. Comp. Vision, pp. 839-846, 1998.
[62] R. Schurch, S. M. Rowland, and T. Starborg, "Serial Block-Face Scanning Electron Microscopy for Three- Dimensional Imaging of Electrical Trees," IEEE Int'l. Conf. Solid Dielectr. (ICSD), pp. 271-274, 2013.
[63] W. Denk and H. Horstmann, "Serial Block-Face Scanning Electron Microscopy to Reconstruct Three-Dimensional Tissue Nanostructure," PLoS Biol, Vol. 2, pp. 1900-1909, 2004.

Roger Schurch (S'11) was born in Temuco, Chile. He received the degree in electrical engineering in 2006 from Santa Maria Technical University, Valparaiso, Chile. He was a high voltage equipment analyst at Transelec transmission company in Santiago, Chile, from 2006-08. He joined the Department of Electrical Engineering, Santa Maria Technical University, as a Junior Lecturer in 2008, where he also carried out dielectric tests for mining and utility companies. Since 2011, he has been a PhD student at the School of Electrical and Electronic Engineering in The University of Manchester. His research project involves the study of electrical trees and partial discharges in polymeric insulation. He was awarded the IEEE Graduate Fellowship of the Dielectrics and Electric Insulation Society in 2011.

Simon M. Rowland (SM'07) was born in London, England. He completed the B.Sc. degree in physics at The University of East Anglia and the Ph.D. degree at London University. He has worked for many years on dielectrics and their applications and has also been Operations and Technical Director within multinational manufacturing companies. He joined The School of Electrical and Electronic Engineering in The University of Manchester as a Senior Lecturer in 2003, and was appointed Professor of Electrical Materials in 2009. He was President of the IEEE Dielectric and Electrical Insulation Society from 2011-12.

Robert S. Bradley was born in St Asaph, UK. He completed BA and MSc degrees in Naturals Sciences (physics) at Cambridge University before gaining a Ph.D. in fluorescence imaging at The University of Manchester. He has since worked as a Postdoctoral Research Associate in Positron Emission Tomography at the Wolfson Molecular Imaging Centre before joining the School of Materials at The University of Manchester in 2008 to help with the setting up of the Henry Moseley X-ray Imaging Facility. His ongoing research interests include the development and application of phase contrast and nano-scale X-ray tomography.

Philip J. Withers was born in Usk, Wales. He completed his BA in Natural Sciences at Cambridge specializing in Theoretical Physics in 1985 and his PhD in 1989 in Materials Science at Cambridge. After 9 years as a Lecturer in Cambridge he took up a Chair in Materials Science at Manchester University in 1998. His work has focused on understanding the performance and structural integrity of engineering materials and components, with particular focus on the effect of residual stresses. In 2009 he set up the Henry Moseley X-ray Imaging Facility at Manchester which has some of the best facilities for computer tomographic imaging of materials in the UK. He is now also Director of the BP International Centre for Advanced Materials.